Nonthyrotoxic Prevention of Diet-Induced Insulin Resistance by 3,5-Diiodo-L-Thyronine in Rats

Pieter de Lange,[1] Federica Cioffi,[2] Rosalba Senese,[1] Maria Moreno,[2] Assunta Lombardi,[3] Elena Silvestri,[2] Rita De Matteis,[4] Lillà Lionetti,[3] Maria Pina Mollica,[3] Fernando Goglia,[2] and Antonia Lanni[1]

OBJECTIVE—High-fat diets (HFDs) are known to induce insulin resistance. Previously, we showed that 3,5-diiodothyronine (T2), concomitantly administered to rats on a 4-week HFD, prevented gain in body weight and adipose mass. Here we investigated whether and how T2 prevented HFD-induced insulin resistance.

RESEARCH DESIGN AND METHODS—We investigated the biochemical targets of T2 related to lipid and glucose homeostasis over time using various techniques, including genomic and proteomic profiling, immunoblotting, transient transfection, and enzyme activity analysis.

RESULTS—Here we show that, in rats, HFD feeding induced insulin resistance (as expected), whereas T2 administration prevented its onset. T2 did so by rapidly stimulating hepatic fatty acid oxidation, decreasing hepatic triglyceride levels, and improving the serum lipid profile, while at the same time sparing skeletal muscle from fat accumulation. At the mechanistic level, *1*) transfection studies show that T2 does not act via thyroid hormone receptor β; *2*) AMP-activated protein kinase is not involved in triggering the effects of T2; *3*) in HFD rats, T2 rapidly increases hepatic nuclear sirtuin 1 (SIRT1) activity; *4*) in an in vitro assay, T2 directly activates SIRT1; and *5*) the SIRT1 targets peroxisome proliferator–activated receptor (PPAR)-γ coactivator (PGC-1α) and sterol regulatory element–binding protein (SREBP)-1c are deacetylated with concomitant upregulation of genes involved in mitochondrial biogenesis and downregulation of lipogenic genes, and PPARα/δ-induced genes are upregulated, whereas genes involved in hepatic gluconeogenesis are downregulated. Proteomic analysis of the hepatic protein profile supported these changes.

CONCLUSIONS—T2, by activating SIRT1, triggers a cascade of events resulting in improvement of the serum lipid profile, prevention of fat accumulation, and, finally, prevention of diet-induced insulin resistance. *Diabetes* 60:2730–2739, 2011

O besity and associated disorders (including insulin resistance, glucose intolerance, dyslipidemia, and hypertension) are approaching epidemic proportions worldwide (1,2). Increasing lipid oxidation in the liver is a key target for improving disturbed glucose homeostasis. Thyroid hormones (THs) are important inducers of both lipid metabolism and metabolic rate by increasing energy expenditure (3), and their potential use as hypolipidemic agents has been considered. However, THs cause a clinical thyrotoxic state—as manifested by cardiac tachyarrhythmia, systolic hypertension, heart failure, and skeletal muscle weakness—that abolishes their usage for this purpose. Instead, current research is focusing on the development of TH analogs that are both tissue and TH receptor (TR) selective (in particular, for the TRβ isoform, which is predominantly involved in TH-induced lipid metabolism) (rev. in 4–7). We recently showed that a natural TH derivative, 3,5-diiodo-L-thyronine (T2), prevents adiposity and body weight gain when administered to rats receiving a high-fat diet (HFD) without unfavorable side effects, usually caused by 3,5,3′-triiodo-L-thyronine (T3), by increasing both energy expenditure and hepatic fatty acid oxidation rate, a process involving AMP-activated protein kinase (AMPK) (8). To investigate whether T2 ameliorates glucose homeostasis, we studied whether and how T2 treatment in rats receiving an HFD would influence lipid accumulation, glucose tolerance, and insulin resistance. Important regulators of lipid/glucose homeostasis include AMPK and the NAD$^+$-dependent deacetylase sirtuin 1 (SIRT1). AMPK is a known metabolic sensor of cellular ATP levels (9), whereas SIRT1 has also emerged as an important regulator of metabolic balance (10–16) that acts in response to an increase in the intracellular NAD$^+$/NADH ratio. To examine whether AMPK and/or SIRT1 triggered the beneficial effects of T2 on energy homeostasis, we studied hepatic AMPK phosphorylation and SIRT1 activity over time, in relation to metabolic parameters and the expression of AMPK/SIRT1 target genes/proteins involved therein, and we evaluated whether T2 was also able to directly activate SIRT1.

RESEARCH DESIGN AND METHODS

Animal experiments. All animals received humane care according to the criteria outlined in the *Guide for the Care and Use of Laboratory Animals* prepared by the National Academy of Sciences and published by the National Institutes of Health. Male Wistar rats (250–300 g) (Charles River Laboratories) were kept one per cage in a temperature-controlled room at 28°C under a 12-h light/12-h dark cycle. Water was available ad libitum. Rats were divided into five groups. The first group (group N) received a standard diet (total metabolizable percentage of energy: 60.4 carbohydrates, 29 proteins, 10.6 fat J/J; 15.88 KJ gross energy/g; Muscedola, Milan, Italy). The second (group HFD) received an HFD (consisting of 280 g diet supplemented with 395 g lyophilized lamb meat [Liomellin, Milan, Italy], 120 g cellulose [Sigma-Aldrich, St. Louis, MO], 20 g mineral mix [ICN Biomedical, Solon, OH], 7 g vitamin mix [ICN], and 200 g low-salt butter [Lurpak, Denmark]) (total metabolizable percentage of energy: 21 carbohydrates, 29 proteins, 50 fat J/J; 19.85 KJ gross energy/g). The third group (group HFD-T2) received the same HFD together with a daily injection of T2 (25 μg/100 g body wt intraperitoneally) (Sigma-Aldrich). Animals in groups N and HFD were sham-injected. In most experiments, animals of the first, second, and third groups were killed at 1 h, 6 h, 1 day, 1 week, 2 weeks, or 4 weeks after the beginning of their diet/treatment schedule. The fourth group [group HFD-(T2)-C] received the above HFD for 1 or 6 h with

a concomitant intraperitoneal injection of T2 (see third group) and/or Compound C (an AMPK inhibitor) (Sigma-Aldrich) at 1 mg/100 g body wt. The fifth group [group HFD-(T2)-EX] received the above HFD for 1 day with a concomitant intraperitoneal injection of T2 (see third group) and/or EX-527 (a SIRT1 inhibitor) (Sigma-Aldrich) at 1 mg/100 g body wt. Body weight and food consumption were monitored throughout the course of treatment (Fig. 1A). At the end of the schedules, rats were anesthetized by an intraperitoneal injection of chloral hydrate (40 mg/100 g body wt) and then killed by decapitation. For each experimental condition, 10 animals were used. Liver, heart, gastrocnemius muscle, and abdominal white adipose tissue were excised, weighed, and either immediately processed for isolation of mitochondria or histochemical analysis or immediately frozen in liquid nitrogen and stored at −80°C for later processing.

Measurements of metabolic parameters. Total body composition analysis was performed as previously reported (17). Respiratory parameters were recorded using an indirect open-circuit calorimeter (Panlab, Cornella, Barcelona, Spain). Measurements were performed every 15 min for 60 min in each cage. The serum levels of cholesterol and triglycerides were determined by standard procedures (18). Plasma adiponectin levels were measured using a commercially available kit (B-Bridge International, Mountain View, CA). Liver and muscle triglyceride contents were determined using an Infinity kit (Sigma-Aldrich). For the oral glucose tolerance test, rats were fasted overnight and then orally dosed with glucose (3 g/kg body wt) dissolved in water. For the insulin tolerance test, rats were fasted for 5 h and then injected intraperitoneally with insulin (homolog rapid-acting, 10 units/kg body wt in sterile saline; Novartis, Basel, Switzerland). Samples of blood were collected before the oral glucose tolerance test and insulin tolerance test and at various times thereafter (as indicated in the figures), and glucose and insulin values were determined by means of a glucose monitor (BRIO, Ascensia, NY), calibrated for use with rats and ELISA (Mercodia rat insulin; Mercodia, Uppsala, Sweden), respectively. In a subgroup of animals, insulin-dependent hepatic AKT phosphorylation was measured 15 min after insulin injection.

Histochemical analysis. Sections of livers were fixed in formol calcium, and 10-μm frozen sections were subsequently stained with Sudan Black B for the detection of fat according to standard procedures. Muscle cryosections (6 μm) were obtained using a cryostat (Leica CM1850) at −29°C and collected onto room-temperature glass slides; then lipid droplets were stained by the neutral lipid dye Oil Red O. Abdominal white adipose tissue (omental depot) was 4% formaldehyde-fixed and paraffin-embedded. The 4-μm-thick sections were obtained and stained by hematoxylin and eosin to assess morphology.

Determination of enzyme activity. Liver nuclei and mitochondria were separated, with the mitochondria being isolated as previously described (19). The rate of mitochondrial fatty acid oxidation was assessed as described previously (19). Total carnitine palmitoyl transferase (CPT) (CPT1 plus CPT2) activity was measured as reported by Alexson and Nedergaard (20). For the in vitro SIRT1 activity assay, 0.1 nmol/L to 1 mmol/L T2 or resveratrol (RSV) was added to purified SIRT1 protein. For the in vivo SIRT1 activity assay, SIRT1 protein was immunoprecipitated in its native form from nuclear extracts prepared according to instructions provided by Millipore (Milan, Italy) using a polyclonal antibody against SIRT1 from Cyclex (Nagano, Japan) and a Catch and Release v2.0 kit from Millipore. Protein concentrations of all samples were determined using the Bio-Rad DC method (Bio-Rad Laboratories). SIRT1 activity was determined as the NAD-dependent and nicotinamide-inhibitable ability of the native isolated SIRT1 protein to deacetylate an acetylated lysine residue linked to a fluorophore using a histone deacetylase assay kit (Abnova, Taiwan, China). To determine whether a given compound caused a nonspecific induction of fluorescence, incubations were included in which the compound was added after stopping the reaction. When used at the maximal concentration (1 mmol/L), RSV caused a nonspecific induction of fluorescence, with values that amounted to not >12% of the total activity induced by RSV. Across the concentration range used here, T2 did not cause any increased fluorescence after addition of the stop solution.

Immunoblotting. Immunoblot analysis was performed as described previously (21). Polyclonal antibodies used for AMPK and phosphorylated AMPK (Thr[172]), acetyl-CoA carboxylase (ACC) (Ser[79]), and Akt/protein kinase B (Akt) and phosphorylated Akt (Ser[473]) were all from Cell Signaling Technology (Beverly, MA); for SIRT1 from Cyclex (Nagano, Japan); for ACC from Upstate Biotechnology (Lake Placid, NY); and for β-actin and tubulin (loading controls) from Sigma-Aldrich and Santa Cruz Biotechnology (Santa Cruz, CA), respectively.

Deacetylation measurements. Liver nuclear extracts (2 mg), isolated as described above, were immunoprecipitated (see above) with polyclonal antibodies against the peroxisome proliferator–activated receptor (PPAR)-γ coactivator (PGC-1α) (Chemicon, Temecula, CA) and sterol regulatory element–binding protein (SREBP)-1c (Santa Cruz), and acetylation of the proteins was measured by immunoblotting using an anti–Ac-Lysine antibody (Cell Signaling).

Cell culture and transient transfection assays. Rat myoblastic L6 cells obtained from the Cell Bank (Interlab Cell Line Collection) of the National Institute for Cancer Research (Genova, Italy) were transfected as described (22). Hormones were added to the medium at concentrations within the range of 0–100 nm.

Gene and protein expression profiling

Quantitative real-time PCR. Quantitative PCR was performed as described previously, on RNA extracted from liver (23).

Proteomic analysis. Protein extracts were prepared from liver of each animal, and each individual protein was assessed separately as described by Silvestri et al. (24). Differentially expressed proteins were identified by means of matrix-assisted laser desorption/ionization time of flight mass spectrometry (MALDI-ToF MS) (25).

Statistical analysis. Results are expressed as means ± SEM. The statistical significance of differences between groups was determined using one-way ANOVA followed by a Student-Newman-Keuls test. Differences were considered significant at $P < 0.05$.

RESULTS

Four weeks of T2 administration prevents HFD-induced changes in systemic metabolic parameters without affecting lean body mass. The lower body weight in HFD-T2 rats versus HFD rats was primarily due to a decrease in adipose mass, since no significant difference in protein gain and muscle was found among the three groups (Fig. 1A). Heart weight, an important thyrotoxicosis marker, did not differ among the groups (ratio heart weight/body weight [mg/g], N: 0.28 ± 0.02, HFD: 0.26 ± 0.003, HFD-T2: 0.25 ± 0.007). Analysis of whole-body O_2 consumption (VO_2) showed that energy expenditure was significantly higher in HFD-T2 rats than in N and HFD rats (Fig. 1A). Furthermore, the respiratory quotient, which reflects the ratio of carbohydrate to fatty acid oxidation, was significantly lower in HFD and HFD-T2 rats than in N rats (Fig. 1A), indicating that HFD and HFD-T2 rats used a relatively greater amount of fatty acids as a fuel source. Serum levels of cholesterol, nonesterified fatty acids, and triglycerides were comparable between HFD-T2 and N animals and were significantly higher in the HFD group than in the other two groups (Fig. 1A). HFD-T2 rats had a better tolerance to a glucose load than HFD rats, and the tolerance of the latter group was comparable to that of N animals at the late time points of the oral glucose tolerance test (Fig. 1B). Insulin tolerance tests revealed that the reduction in glucose due to insulin administration was comparable between HFD-T2 and N animals, but was impaired in HFD animals (Fig. 1B). These results reveal that the development of insulin resistance during HFD feeding can be prevented by T2 administration.

Four weeks of T2 administration prevents HFD-induced changes in ectopic fat accumulation through increased hepatic mitochondrial fatty acid oxidation. After 4 weeks of treatment, T2 had prevented fat storage in the tissues predominantly involved in lipid and glucose homeostasis (such as gastrocnemius muscle, abdominal white adipose tissue, and liver), as revealed by histological analysis (Fig. 1C). Accordingly, accumulation of triglyceride in muscle and liver was prevented (Fig. 1D), as was the hypertrophy of white adipocytes (Fig. 1C). Mitochondrial fatty acid oxidation was unaltered in gastrocnemius (Fig. 1E), soleus, and extensor digitorum longus muscle (values [nmoles oxygen/mg protein × min] for soleus: N: 28.02 ± 5.1, HFD: 28.92 ± 3.3, HFD-T2: 26.89 ± 4.21; and for extensor digitorum longus: N: 24.81 ± 2.2, HFD: 48.23 ± 3.6, HFD-T2: 57.52 ± 5.3). T2 treatment increased hepatic mitochondrial fatty acid oxidation (Fig. 1E), which indicates that the liver drives T2-induced systemic fat depletion, consistent with an increased hepatic phosphorylation of AMPK (Thr[172]) with respect to HFD animals (Fig. 1F).
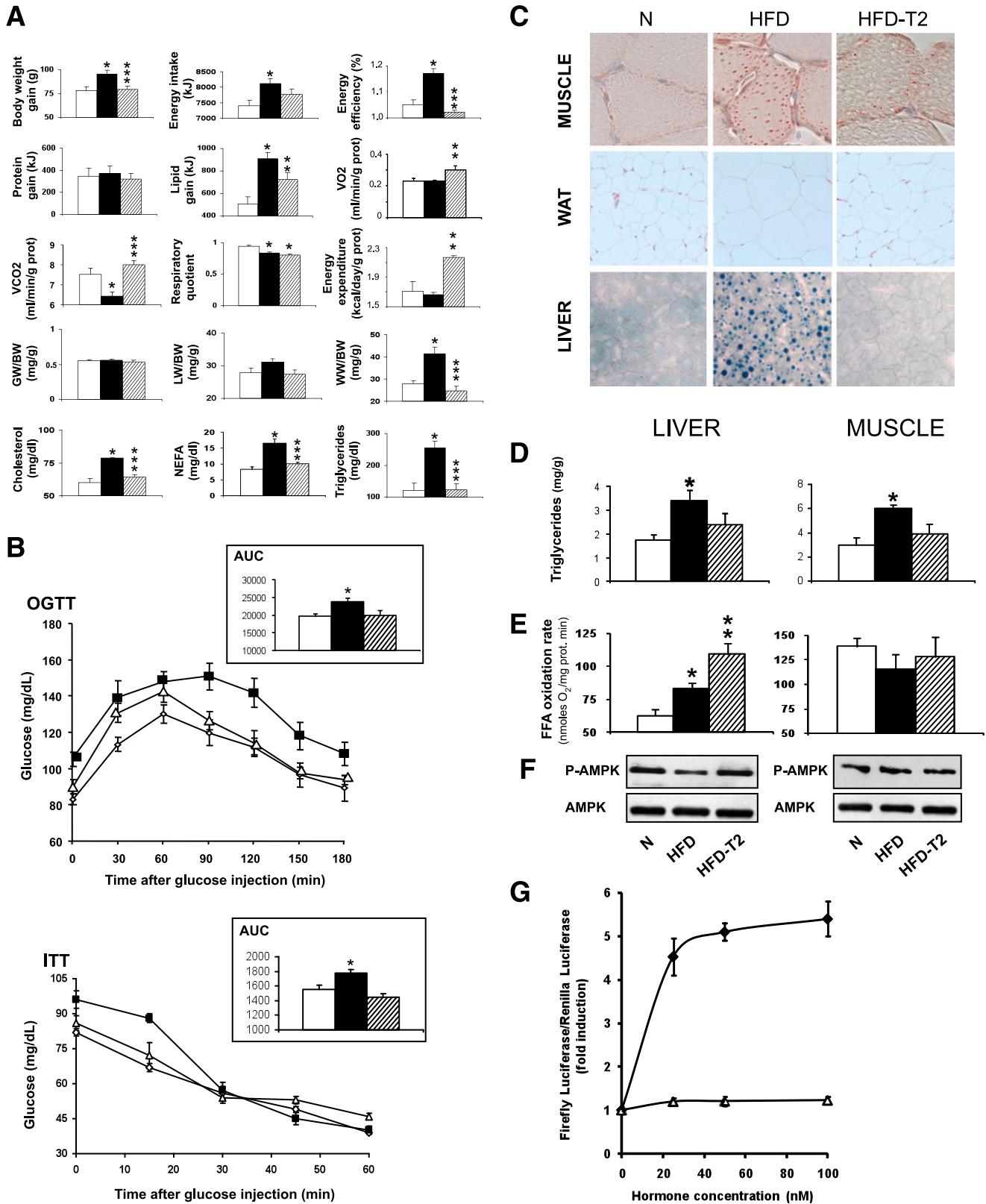
FIG. 1. Four weeks of T2 administration prevents HFD-induced changes in systemic metabolic parameters and fat accumulation, independently of TRβ. *A*: T2 normalizes HFD-altered metabolic parameters and *B*: glucose tolerance (*upper*) and insulin resistance (*lower*). *Upper and lower insets*: area under the curve (AUC). *C–F*: T2 prevents fat (*C*) and triglyceride (*D*) accumulation and increases mitochondrial fatty acid oxidation (*E*) and phosphorylation of AMPK (Thr^{172}) (*F*) in the indicated tissues. *G*: In contrast to T3, T2 does not activate the human uncoupling protein 3 promoter through interaction with TRβ in transiently transfected rat L6 myotubes. Error bars represent SEM. *$P < 0.05$ vs. untreated controls; **$P < 0.05$ vs. both untreated controls and HFD-fed groups; ***$P < 0.05$ vs. HFD-fed group. Energy efficiency = body weight gain/metabolized energy intake. BW, body weight; GW, gastrocnemius weight; LW, liver weight; NEFA, nonesterified fatty acids; prot, protein; VCO$_2$, carbon dioxide production; WW, white adipose weight. Vo$_2$ and energy expenditure are normalized to lean body weight. *A–E*: □/◇ = N; ■ = HFD; ▨/△ = HFD-T2. *G*: ◆ = T2, △ = T3. (A high-quality color representation of this figure is available in the online issue.)
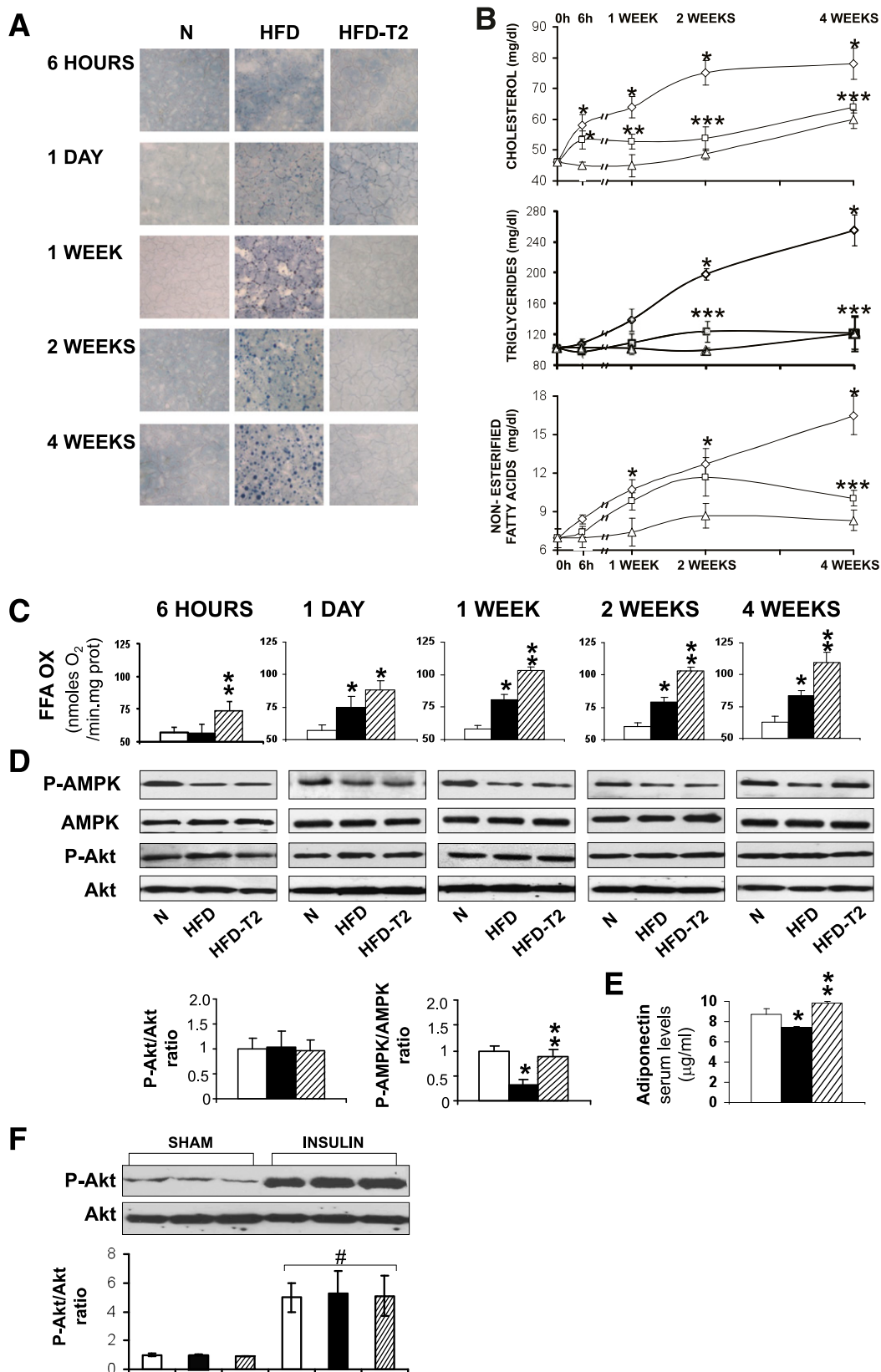
FIG. 2. T2 rapidly prevents hepatic and serum fat accumulation. *A*: Hepatic fat accumulation (assessed by Sudan black staining) is prevented by T2 administration to rats simultaneously fed an HFD. *B*: T2 rapidly normalizes levels of nonesterified fatty acids, triglycerides, and cholesterol. Levels were measured at the indicated time points after T2 injection. *C*: Hepatic mitochondrial fatty acid oxidation (FFA OX) rapidly increases in response to T2 treatment. *D*: Phosphorylation of AMPK (Thr[172]) increases only after 4 weeks of T2 treatment, and phosphorylation of Akt (Ser[473]) does not change in response to T2 treatment. Representative blots are shown. The histograms represent values obtained after 4 weeks of treatment. *E*: T2 normalizes serum adiponectin levels. *F*: After 4 weeks, neither HFD nor HFD-T2 treatment alters insulin-induced hepatic Akt (Ser[473]) phosphorylation with respect to controls (N). Error bars represent SEM. *$P < 0.05$ vs. untreated controls; **$P < 0.05$ vs. both untreated controls and HFD-fed groups; ***$P < 0.05$ vs. HFD-fed group; #$P < 0.05$ vs. sham-injected animals. *B*: △, N; ◇, HFD; □, HFD-T2. *C–F*: □, N; ■, HFD; ▨, HFD-T2; prot, protein. (A high-quality color representation of this figure is available in the online issue.)
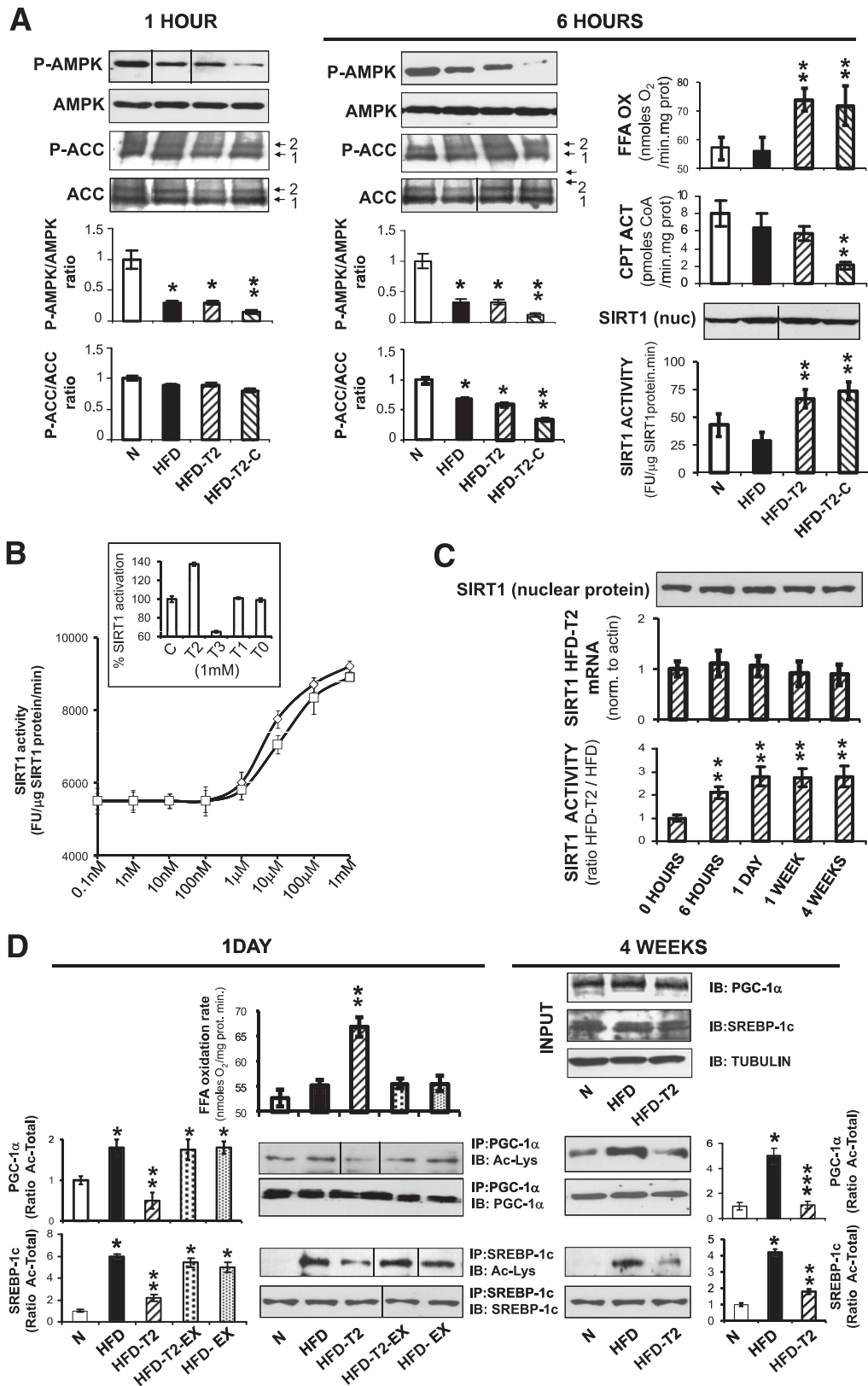
FIG. 3. Hepatic induction of fatty acid oxidation by T2 in HFD animals does not involve AMPK but is associated with SIRT1 activation. *A*: Compound C effectively inhibits AMPK Thr[172] and ACC Ser[79] phosphorylation within 1 and 6 h, respectively, of its simultaneous administration with T2. Positions of ACC isoforms 1 and 2 are indicated at the right. The increase of fatty acid oxidation persisted at 6 h after injection of T2 plus Compound C. SIRT1 nuclear protein activity increased at 6 h after injection of T2 and was not inhibited by Compound C. *B*: T2 is a specific activator of SIRT1. The effects of T2 and RSV (positive control) were compared using a fluorescence-based deacetylation assay (*x*-axis: logarithmic scale). *Inlay*: Other tested TH metabolites either inhibit SIRT1 activity (T3) or are ineffective (T1, T0). *C*: T2 induces prolonged activation of SIRT1. *Upper*: Nuclear SIRT1 protein. *Middle*: mRNA levels in livers of animals treated as indicated underneath the bars. *Lower*: Hepatic nuclear SIRT1 activity. Ratios are shown for values from HFD-T2 animals over those from HFD animals at the indicated time points. *D*: T2 treatment causes

T2 does not directly elicit transcription through TH receptor β. Because the transcriptional effects of T3 on lipid metabolism are predominantly exerted through TRβ (7), we asked whether the phenotype observed above was due to T2 directly affecting transcription through TRβ. To address this question, we performed a cotransfection experiment using rat L6 myoblasts. A luciferase expression vector containing the human uncoupling protein 3 (UCP3) promoter, a known target of T3 through TRβ (22,26), was cotransfected with two expression vectors containing the human thyroid hormone receptor β (hTRβ) and myoblast determination protein 1 (MyoD), respectively. In the presence of 25 nmol/L T3, luciferase activity increased sharply to 4.5-fold versus control, while in the presence of 100 nmol/L T3, luciferase activity values reached 5.5-fold versus control (Fig. 1G). Across the concentration range used here (0–100 nmol/L for each hormone), T2 did not significantly increase luciferase activity, showing that the effects of T2 described above are not mediated via increased transcription of target genes through TRβ.

T2 rapidly prevents hepatic and serum fat accumulations. A 6-h exposure to the HFD already induced a substantial lipid-droplet accumulation. In contrast, this effect was lacking in the HFD-T2 group at that time point (Fig. 2A) and indeed at time points of up to 4 weeks (maximum treatment period) (Fig. 2A). Importantly, T2 treatment consistently prevented the HFD-dependent increases in serum cholesterol, triglycerides, and nonesterified fatty acids (Fig. 2B). Accordingly, mitochondrial free fatty acid oxidation was already elevated by T2 at the 6-h time point, and this increase persisted throughout the treatment period (Fig. 2C). We did not observe increases in AMPK phosphorylation in the HFD-T2 rats in the investigated time points up to 2 weeks of treatment. Actually, AMPK phosphorylation was lower in the HFD and HFD-T2 rats than in the N controls. Only after 4 weeks of treatment was there a T2-induced increase in AMPK phosphorylation toward N levels (Fig. 2D), and at that time point, plasma adiponectin levels were elevated, too (Fig. 2E). Basal hepatic Akt phosphorylation (Ser[473]) did not change during feeding on the HFD (Fig. 2D), and it was not inhibited in response to insulin after 4 weeks of HFD treatment (Fig. 2F). T2 had no apparent effect on this result. The plasma ALT level, well documented as a marker of hepatocyte damage, was significantly ($P < 0.05$) elevated in HFD rats, whereas administration of T2 to HFD rats prevented this increase (actual values: 38 ± 1.3, 47 ± 2.0, and 36 ± 1.0 units/L for N, HFD, and HFD-T2 groups, respectively).

Rapid induction of hepatic fatty acid oxidation by T2 in HFD animals involves not AMPK, but SIRT1 activation. To examine whether a transient phosphorylation of AMPK between 0 and 6 h might have triggered the observed T2-induced increase in liver fatty acid oxidation, we concomitantly administered T2 and Compound C to a subgroup of HFD animals. There was an almost complete inhibition of AMPK phosphorylation by Compound C at both 1 and 6 h after T2 injection (Fig. 3A, *left and center panels*). However, the T2-induced increase in mitochondrial fatty acid oxidation in the liver was not different between the HFD-T2–Compound C and HFD-T2 groups (Fig. 3A, *far right upper panel*), although CPT activity was significantly lower in the former group than in all other conditions examined (Fig. 3A, *far right center panel*). Besides AMPK, SIRT1 has emerged as an interesting target in the amelioration of diet-induced metabolic disorders. To examine the involvement of SIRT1 in the effects brought about by T2 in vivo, we isolated hepatic nuclei and immunoprecipitated nuclear SIRT1 protein under native conditions. In agreement with the rapid preventive effect of T2 on fat accumulation, in the HFD-T2 group, hepatic SIRT1 activity was already elevated at the 6-h time point by around twofold versus the HFD group (Fig. 3A, *far right lower panel*). A quantitatively similar result was obtained for the HFD-T2–Compound C group, showing that the activating effect of T2 on SIRT1 is AMPK independent (Fig. 3A, *far right lower panel*). We then examined whether T2 could directly activate purified SIRT1. For this, we used a fluorescence-based deacetylation assay, with the naturally occurring SIRT1 activator RSV as a positive control. The half-maximal inhibitory concentration (IC$_{50}$) values were 8.5 and 17 μmol/L for RSV and T2, respectively, with both activities being inhibitable by nicotinamide (Fig. 3B). Other iodothyronines (T1 and T0) did not stimulate SIRT1 activity at concentrations of 1 mmol/L, whereas T3 inhibited it (see inlay, Fig. 3B). With time, The SIRT1-activity ratio between the HFD-T2 and HFD groups remained elevated (at around two- to threefold vs. control) (up to 4 weeks) (Fig. 3C, *lower*). In the HFD-T2 group, SIRT1 nuclear protein levels did not alter significantly with time (Fig. 3C, *upper*), nor did SIRT1mRNA levels (Fig. 3C, *middle*). HFD treatment caused acetylation of SIRT1 targets SREBP-1c and PGC-1α, which was effectively prevented by T2 coadministration (Fig. 3D). Overnight inhibition of SIRT1 activity with EX-527 abolished T2-induced mitochondrial fatty acid oxidation (Fig. 3D, *left upper panel*) as well as deacetylation of SREBP-1c and PGC-1α (Fig. 3D, *left lower panel*).

T2 shifts hepatic gene and protein-expression profiles toward increased lipid handling and decreased gluconeogenesis, associated with "early" SIRT1- and "late" SIRT1/AMPK-induced increases in cell signaling. The effects of T2 through SIRT1 clearly involve inhibition of lipogenesis and increased mitochondrial activity, through deacetylation of SREBP-1c and PGC-1α. Acetylated SREBP-1c induces transcription of critical lipogenic genes, and we found that after 2 weeks in the HFD-T2 animals, the SREBP-1c target genes *ACC* and fatty acid synthase (*FAS*) were downregulated (Fig. 4A). A third gene involved in lipogenesis, Spot 14 (*S14*), was also downregulated by T2, and a lipolytic gene, hepatic lipase (*HL*), involved in downregulation of triglycerides, was upregulated (Fig. 4A). Regarding mitochondrial biogenesis, T2 deacetylated PGC-1α but did not increase *PGC-1α* gene expression, and neither

---

deacetylation of SIRT1 target proteins, consistent with increased fatty acid oxidation. *Left panel*: Mitochondrial fatty acid oxidation in HFD or HFD-T2 animals treated for 1 day (*left panel*) in the presence or absence of the specific SIRT1 inhibitor EX-527 (EX). *Left and right panel*: In the same animals, as well as in animals treated for 4 weeks, hepatic nuclear extracts (2 mg) were immunoprecipitated with an anti–PGC-1α (*upper*) or anti–SREBP-1c antibody (*lower*) and analyzed with anti-acetyllysine antibody vs. PGC-1α or SREBP-1c. Numbers indicate the ratio acetylated over total protein. *Upper right panel*: No variation in total PGC-1α, SREBP-1c, and tubulin (control) protein levels in nuclear extracts between N, HFD, and HFD-T2 animals (input). *A*, *C*, and *D*: Representative blots are shown. *D*: Dividing lines indicate omissions/rearrangements of lanes from the same gel. Error bars represent SEM. *$P < 0.05$ vs. untreated controls; **$P < 0.05$ vs. both untreated controls and HFD-fed groups. □, N; ■, HFD; ▨, HFD-T2; ▩, HFD-T2–Compound C; dotted bars, HFD-T2-EX-527; light dotted bars, HFD-EX-527. *B*: ◇, RSV; □, T2. FFA, free fatty acid; FU, fluorescence units; IP, immunoprecipitated; IB, immunoblotted.

that of nuclear respiratory factors 1 and 2 (*NRF1* and *NRF2*). However, those of mitochondrial transcription factor A and cytochrome oxidase subunit IV were increased in the HFD-T2 animals (Fig. 4*B*). Because fatty acid oxidation is known to be governed by PPARα and PPARδ in the liver, we measured the expression of *PPARα* and *PPARδ*, as well as the expression of a number of known *PPARα/δ* target genes. PPARs were targets of both AMPK and SIRT1, and gene expression was measured at both the 2-week time point (when only SIRT1 activity was increased) and the 4-week time point (when both SIRT1 and AMPK activities were increased). The PPARα/δ target genes were as follows: *CPT1a* and *CPT2* (each involved in mitochondrial fatty acid uptake), acyl-CoA oxidase (*AOX*; a key enzyme in peroxisomal fatty acid oxidation), uncoupling protein 2 (*UCP2*; a PPAR target gene that is not translated into protein in the liver), and mitochondrial thioesterase I (*MTE I*; involved in mitochondrial lipid handling). In addition, because glucose tolerance was significantly ameliorated in HFD-T2 rats, we measured the expression of key genes in glucose homeostasis, which have been shown to be targets of AMPK and SIRT1. These key genes were as follows: phosphoenolpyruvate carboxykinase (*PEPCK*; which converts oxaloacetate to phosphoenolpyruvate and carbon dioxide), liver pyruvate kinase (*LPK*; a glycolytic enzyme that converts phosphoenolpyruvate to pyruvate), and glucose-6-phosphatase (*G6Pase*; which converts glucose-6-phosphate to glucose, which is then released from the hepatocyte). At 2 weeks, HFD-T2 rats displayed (vs. HFD rats) the following: *1*) increased expression of *PPARα*, but not of *PPARδ* (Fig. 4*C*); *2*) significant upregulation of the expression of *CPT1a* and *CPT2* (Fig. 4*D*); and *3*) significant reductions in the expression of *LPK* and *G6Pase* (Fig. 4*E*). At 4 weeks (again vs. HFD animals), HFD-T2 animals displayed significantly increased expression of both *PPARα* and *PPARδ* (Fig. 4*F*) and of all the above-mentioned PPARα/δ target genes (Fig. 4*G*). The expression of *LPK* and *G6Pase* were downregulated (as at 2 weeks), and that of *PEPCK* was still unaltered by T2 (Fig. 4*H*). Subsequently, we performed a high-resolution differential proteomic analysis on livers from N, HFD, and HFD-T2 rats. From the spots showing differential expression among the three analyzed groups, nine protein spots were identified and selected as proteins involved in glucose or lipid metabolism (Fig. 4*I* and *J* and Table 1). T2 treatment *1*) prevented the induced elevations in glycolytic (LPK) and gluconeogenic (PEPCK, fructose-1,6-bisphosphatase 1 [FBPase1], and isocitrate dehydrogenase [IDH]) enzymes (Fig. 4*I* and Table 1), *2*) had a strong positive impact on the expression of enzymes involved in fatty acid oxidation (enoyl CoA hydratase [ECH]), and *3*) had normalizing effects on lipogenic proteins (carbonic anhydrase 3 [CA3] and glycerol-3-phosphate dehydrogenase [GPDH]) (Fig. 4*J* and Table 1).

DISCUSSION

Coadministration of T2 to HFD-fed rats protects against fat accumulation and the resulting insulin resistance, primarily by promoting hepatic fat consumption, thereby avoiding a serum lipid increase. We identify SIRT1 as a main target recruited in mediating the effects of T2 and exclude a triggering role for the AMPK-ACC-CPT axis under the present conditions. We further found that T2 does not act through TRβ (involved in the TH-mediated regulation of lipid metabolism [7,27]). TH derivatives GC-1 (soberitome) and KB2115 (eprotirome) show hypolipidemic effects similar

to those provoked by T2, and clinical trials are now in progress (4,5). By acting through TRβ, however, they reduce serum thyrotropin and thyroxine levels in animals with potencies similar to those of their beneficial cholesterol-lowering effects (5), whereas T2 does not (8). The increase in liver mitochondrial fatty acid oxidation induced by T2 was rapid in onset, preventing the HFD-induced rise in serum lipid parameters. The early significant stimulation of hepatic fatty acid oxidation and inhibition of lipogenesis by T2 leads to *1*) prevention of hepatic fat accumulation, *2*) a consequent absence of increases in the serum lipid concentration, *3*) a blockage of delivery of fat to the muscle and unaltered fatty acid oxidation in various muscles, and *4*) at least in part, decreased delivery of fat into adipocytes. Given the well-known dangerous effects of ectopic fat accumulation on insulin sensitivity, the above actions of T2 on lipid handling counteract the HFD-induced insulin resistance. Whereas several observations support the idea that AMPK and SIRT1 act in concert to ensure an appropriate cellular response and adaptation to environmental modifications (28,29), others have shown that SIRT1 can also act independent of AMPK (16), and our present results are in favor of this. SIRT1 has recently been shown to be crucial for hepatic lipid homeostasis (30,31) and acts in cooperation with other factors to improve insulin sensitivity. Hepatic SIRT1 knockout animals exhibit lower basal hepatic Akt phosphorylation levels (30), which those authors interpreted as a sign of decreased insulin sensitivity. However, in the current study, we did not observe a T2-mediated increase in Akt/PKB (protein kinase B) phosphorylation (Ser[473]) during feeding on the HFD, neither in the absence nor in the presence of insulin. Interestingly, mice overexpressing SIRT1 display enhanced hepatic insulin sensitivity, an effect that correlates with an increase in plasma adiponectin (32), which is in accordance with the increase the plasma adiponectin level by T2. In line with the above, the action of T2, through deacetylation of SIRT1 targets SREBP-1c and PGC-1α (16,31), involves genetic reprogramming of lipid/glucose utilization and mitochondrial biogenesis, as well as an enhancement of PPARα/δ signaling. *SIRT1* mRNA levels themselves were not altered. Importantly, the expression of *G6Pase* and *LPK* were decreased, which would result in reductions in both glucose release and glycolysis, and contribute to the improved glucose tolerance brought about by T2 administration. Proteomic analysis confirmed several of these changes in gene expression and also revealed post-transcriptional modifications. For instance, whereas the mRNA level of *PEPCK* remained unaltered after up to 4 weeks of T2 treatment, the protein was clearly downregulated, as were other proteins involved in gluconeogenesis, thus showing that gluconeogenesis can be inhibited by T2 in the liver in rats on an HFD. Moreover, the T2-induced downregulation of *LPK* suggested a decreased glycolysis in the liver in HFD-T2 rats. In addition, T2 markedly reduced the protein expression levels of enzymes such as CA3 (involved in hepatic de novo lipogenesis [33]) and GPDH (involved in triacilglycerol formation) while increasing the expression of proteins involved in fatty acid oxidation (such as enoyl-CoA hydratase). These effects would contribute to the antisteatotic effect of T2 (34).

In summary, this study demonstrates that *1*) T2 prevents HFD-induced insulin resistance and glucose intolerance; *2*) it does so by directly activating SIRT1 in an AMPK-independent manner, blocking accumulation of ingested fat in the liver; *3*) this effect is reflected by a reduction in
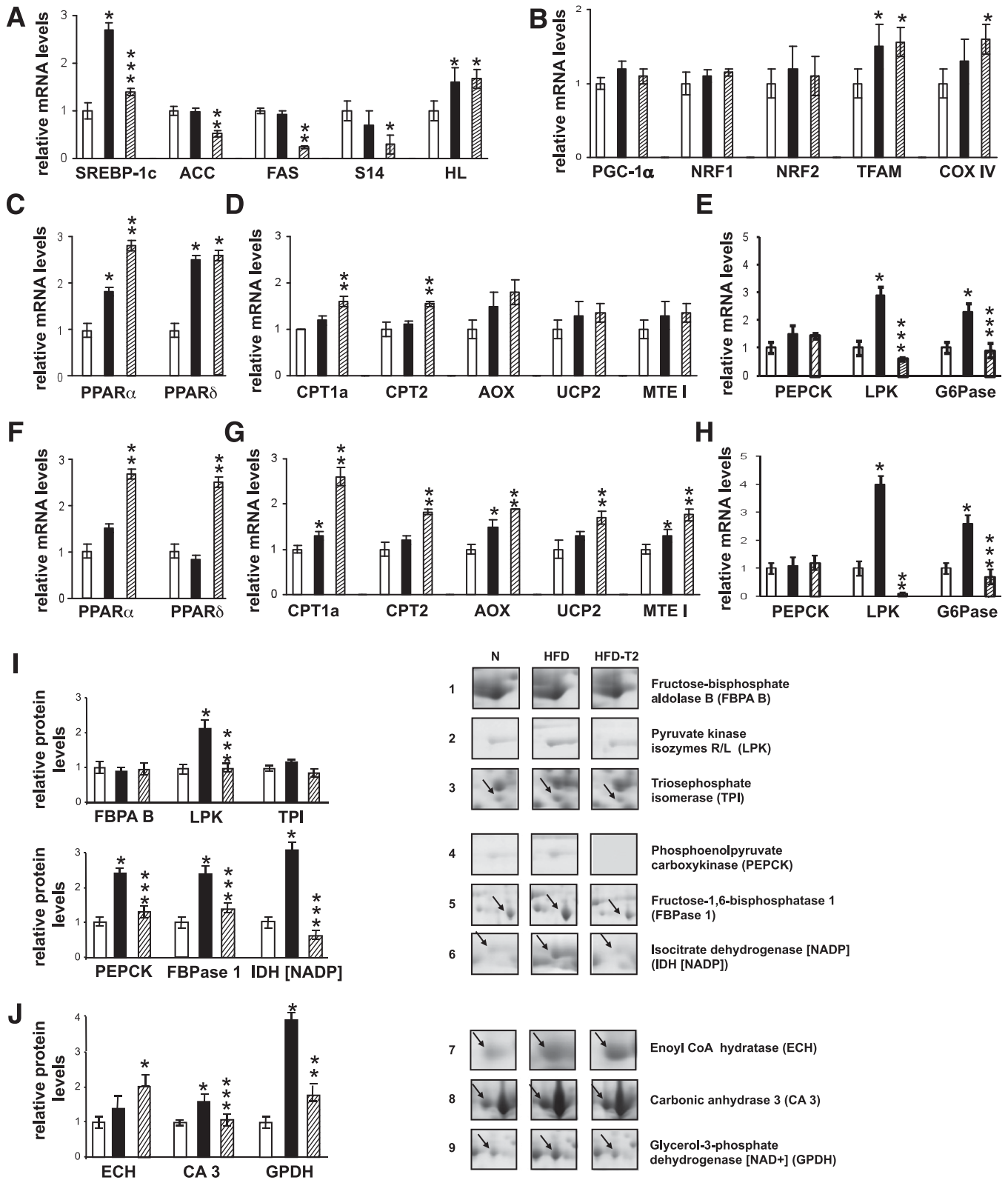
FIG. 4. T2 shifts hepatic gene and protein expression profiles toward increased lipid handling and decreased lipogenesis and gluconeogenesis. *A–H*: Quantitative RT-PCR analysis showing that T2 modulates gene expression in favor of lipid reduction (*A*), increases expression of genes involved in mitochondrial biogenesis (*B*), increases PPARα/δ expression (*C* and *F*), and genes involved in hepatic fatty acid oxidation (*D* and *G*), and normalizes the expression of genes involved in glucose homeostasis (*E* and *H*), after 2 weeks (*A–E*) or 4 weeks (*F–H*) of HFD-T2 treatment. Expression was normalized to that of Cyclophilin F. *I* and *J*: Proteomic analysis revealed protein profile changes toward adjustment of hepatic glucose metabolism (*I*) and lipid metabolism (*J*) to the HFD challenge. *Left*: Quantification of the data (for each treatment, expressed relative to the value obtained for control [N] rats, which was set as 1.0). *Right*: Representative 2D-E subsections obtained from livers of N, HFD, and HFD-T2 (4 weeks) rats. Error bars represent SEM. *$P < 0.05$ vs. untreated controls; **$P < 0.05$ vs. both untreated controls and HFD-fed groups; ***$P < 0.05$ vs. HFD-fed group. □, N; ■, HFD; ▨, HFD-T2.

TABLE 1
Differentially expressed proteins in liver of HFD-T2 versus HFD rats, as assessed by proteomic analysis

Spot number	Protein name	Protein function	Accession number	Theoretical isoelectric point/molecular mass (kDa)	Probability	Matches
		Glycolysis				
1	Fructose-bisphosphate aldolase B (FBPA)	Carbohydrate degradation	P00884	8.43/39.8	3.0E-09	9
2	Pyruvate kinase isozymes R/L (LPK)	Carbohydrate degradation	P00884	6.90/62.5	3.4E-10	9
3	Triosephosphate isomerase (TPI)	Carbohydrate degradation	P48500	6.84/27.3	1.3E-09	7
		Gluconeogenesis				
4	PEPCK	Rate-limiting step in the metabolic pathway that produces glucose	P07379	6.46/70.1	2.1E-07	8
5	Fructose-1,6-bisphosphatase 1 (FBPase1)	Carbohydrate biosynthesis	P19112	5.56/39.9	7.0E-11	8
6	Isocitrate dehydrogenase [NADP] (IDH)	Production of NADPH	P41562	6.99/47.0	9.0E-6	6
		Lipid metabolism (mitochondrial β-oxidation)				
7	Enoyl CoA hydratase (ECH)	Mitochondrial fatty acid β-oxidation	P14604	8.1/31.8	3.3E-08	7
		Lipid metabolism (lipogenesis)				
8	Carbonic anhydrase 3 (CA3)	Hydration of carbon dioxide; major participant in the hepatic response to oxidative stress	P14141	6.99/29.5	2.0E-09	7
9	Glycerol-3-phosphate dehydrogenase [NAD+] (GPDH)	Triglyceride biosynthesis	O35077	6.76/37.8	8.0E-08	8

the circulating levels of cholesterol and triglycerides; and *4*) under these conditions, T2 specifically augments liver metabolic activity, thus "sparing" skeletal muscle. Because side effects are minimized, this natural thyroid-hormone metabolite can convey a favorable effect on metabolism-associated diseases.

REFERENCES

1. Reilly MP, Rader DJ. The metabolic syndrome: more than the sum of its parts? Circulation 2003;108:1546–1551
2. Barness LA, Opitz JM, Gilbert-Barness E. Obesity: genetic, molecular, and environmental aspects. Am J Med Genet A 2007;143A:3016–3034
3. Oppenheimer JH, Schwartz HL, Lane JT, Thompson MP. Functional relationship of thyroid hormone-induced lipogenesis, lipolysis, and thermogenesis in the rat. J Clin Invest 1991;87:125–132
4. Moreno M, de Lange P, Lombardi A, Silvestri E, Lanni A, Goglia F. Metabolic effects of thyroid hormone derivatives. Thyroid 2008;18:239–253
5. Baxter JD, Webb P. Thyroid hormone mimetics: potential applications in atherosclerosis, obesity and type 2 diabetes. Nat Rev Drug Discov 2009;8: 308–320
6. Cioffi F, Lanni A, Goglia F. Thyroid hormones, mitochondrial bioenergetics and lipid handling. Curr Opin Endocrinol Diabetes Obes 2010;17:402–407
7. Ribeiro MO. Effects of thyroid hormone analogs on lipid metabolism and thermogenesis. Thyroid 2008;18:197–203
8. Lanni A, Moreno M, Lombardi A, et al. 3,5-Diiodo-L-thyronine powerfully reduces adiposity in rats by increasing the burning of fats. FASEB J 2005; 19:1552–1554
9. Hardie DG. AMP-activated/SNF1 protein kinases: conserved guardians of cellular energy. Nat Rev Mol Cell Biol 2007;8:774–785
10. Baur JA, Pearson KJ, Price NL, et al. Resveratrol improves health and survival of mice on a high-calorie diet. Nature 2006;444:337–342
11. Gerhart-Hines Z, Rodgers JT, Bare O, et al. Metabolic control of muscle mitochondrial function and fatty acid oxidation through SIRT1/PGC-1alpha. EMBO J 2007;26:1913–1923
12. Lagouge M, Argmann C, Gerhart-Hines Z, et al. Resveratrol improves mitochondrial function and protects against metabolic disease by activating SIRT1 and PGC-1alpha. Cell 2006;127:1109–1122
13. Picard F, Kurtev M, Chung N, et al. Sirt1 promotes fat mobilization in white adipocytes by repressing PPAR-gamma. Nature 2004;429:771–776
14. Rodgers JT, Lerin C, Haas W, Gygi SP, Spiegelman BM, Puigserver P. Nutrient control of glucose homeostasis through a complex of PGC-1alpha and SIRT1. Nature 2005;434:113–118
15. Rodgers JT, Puigserver P. Fasting-dependent glucose and lipid metabolic response through hepatic sirtuin 1. Proc Natl Acad Sci U S A 2007;104: 12861–12866
16. Feige JN, Lagouge M, Cantò C, et al. Specific SIRT1 activation mimics low energy levels and protects against diet-induced metabolic disorders by enhancing fat oxidation. Cell Metab 2008;8:347–358
17. Lionetti L, Mollica MP, Crescenzo R, et al. Skeletal muscle subsarcolemmal mitochondrial dysfunction in high-fat fed rats exhibiting impaired glucose homeostasis. Int J Obes (Lond) 2007;31:1596–1604

18. Mollica MP, Lionetti L, Moreno M, et al. 3,5-Diiodo-l-thyronine, by modulating mitochondrial functions, reverses hepatic fat accumulation in rats fed a high-fat diet. J Hepatol 2009;51:363–370

19. Moreno M, Lanni A, Lombardi A, Goglia F. How the thyroid controls metabolism in the rat: different roles for triiodothyronine and diiodothyronines. J Physiol 1997;505:529–538

20. Alexson SEH, Nedergaard J. A novel type of short- and medium-chain acyl-CoA hydrolases in brown adipose tissue mitochondria. J Biol Chem 1988; 263:13564–13571

21. de Lange P, Farina P, Moreno M, et al. Sequential changes in the signal transduction responses of skeletal muscle following food deprivation. FASEB J 2006;20:2579–2581

22. de Lange P, Feola A, Ragni M, et al. Differential 3,5,3′-triiodothyronine-mediated regulation of uncoupling protein 3 transcription: role of Fatty acids. Endocrinology 2007;148:4064–4072

23. Senese R, Valli V, Moreno M, et al. Uncoupling protein 3 expression levels influence insulin sensitivity, fatty acid oxidation, and related signaling pathways. Pflugers Arch 2011;461:153–164

24. Silvestri E, Moreno M, Schiavo L, et al. A proteomics approach to identify protein expression changes in rat liver following administration of 3,5,3′-triiodo-L-thyronine. J Proteome Res 2006;5:2317–2327

25. Lombardi A, Silvestri E, Cioffi F, et al. Defining the transcriptomic and proteomic profiles of rat ageing skeletal muscle by the use of a cDNA array, 2D- and Blue native-PAGE approach. J Proteomics 2009;72: 708–721

26. Solanes G, Pedraza N, Iglesias R, Giralt M, Villarroya F. The human uncoupling protein-3 gene promoter requires MyoD and is induced by retinoic acid in muscle cells. FASEB J 2000;14:2141–2143

27. Cable EE, Finn PD, Stebbins JW, et al. Reduction of hepatic steatosis in rats and mice after treatment with a liver-targeted thyroid hormone receptor agonist. Hepatology 2009;49:407–417

28. Fulco M, Sartorelli V. Comparing and contrasting the roles of AMPK and SIRT1 in metabolic tissues. Cell Cycle 2008;7:3669–3679

29. Cantó C, Jiang LQ, Deshmukh AS, et al. Interdependence of AMPK and SIRT1 for metabolic adaptation to fasting and exercise in skeletal muscle. Cell Metab 2010;11:213–219

30. Purushotham A, Schug TT, Xu Q, Surapureddi S, Guo X, Li X. Hepatocyte-specific deletion of SIRT1 alters fatty acid metabolism and results in hepatic steatosis and inflammation. Cell Metab 2009;9:327–338

31. Ponugoti B, Kim D-H, Xiao Z, et al. SIRT1 deacetylates and inhibits SREBP-1C activity in regulation of hepatic lipid metabolism. J Biol Chem 2010;285: 33959–33970

32. Banks AS, Kon N, Knight C, et al. SirT1 gain of function increases energy efficiency and prevents diabetes in mice. Cell Metab 2008;8:333–341

33. Lynch CJ, Fox H, Hazen SA, Stanley BA, Dodgson S, Lanoue KF. Role of hepatic carbonic anhydrase in de novo lipogenesis. Biochem J 1995;310: 197–202

34. Supuran CT, Di Fiore A, De Simone G. Carbonic anhydrase inhibitors as emerging drugs for the treatment of obesity. Expert Opin Emerg Drugs 2008;13:383–392